BIOCHEMISTRY
including biophysical chemistry & molecular biology

Article

pubs.acs.org/biochemistry

Conformational Basis for Substrate Recruitment in Protein Tyrosine Phosphatase 10D

Lalima L. Madan and B. Gopal*

Molecular Biophysics Unit, Indian Institute of Science, Bangalore 560 012, India

Supporting Information

ABSTRACT: The coordinated activity of protein tyrosine phosphatases (PTPs) is crucial for the initiation, modulation, and termination of diverse cellular processes. The catalytic activity of this protein depends on a nucleophilic cysteine at the active site that mediates the hydrolysis of the incoming phosphotyrosine substrate. While the role of conserved residues in the catalytic mechanism of PTPs has been extensively examined, the diversity in the mechanisms of substrate recognition and modulation of catalytic activity suggests that other, less conserved sequence and structural features could contribute to this process. Here we describe the crystal structures of *Drosophila melanogaster* PTP10D in the apo form as well as in a complex with a substrate peptide and an inhibitor. These studies reveal the role of aromatic ring stacking interactions at the boundary of the active site of PTPs in mediating substrate recruitment. We note that phenylalanine 76, of the so-called KNRY loop, is crucial for orienting the phosphotyrosine residue toward the nucleophilic cysteine. Mutation of phenylalanine 76 to leucine results in a 60-fold decrease in the catalytic efficiency of the enzyme. Fluorescence measurements with a competitive inhibitor, *p*-nitrocatechol sulfate, suggest that Phe76 also influences the formation of the enzyme−substrate intermediate. The structural and biochemical data for PTP10D thus highlight the role of relatively less conserved residues in PTP domains in both substrate recruitment and modulation of reaction kinetics.

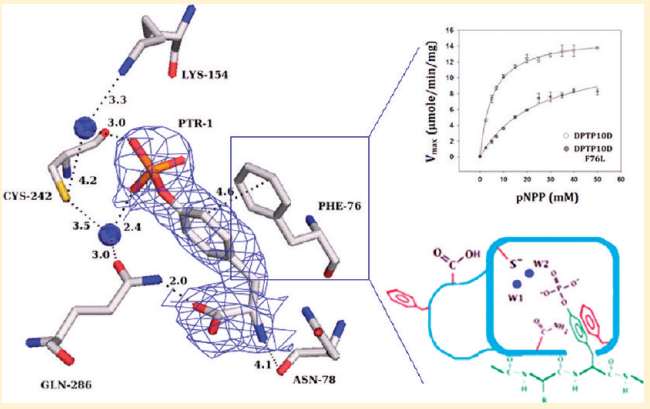

Protein tyrosine phosphatases (PTPs) are key regulators of various signaling processes and are crucial for the balance of phosphorylated tyrosines in maintaining cellular homeostasis.[1] Forming the reverse switch for tyrosine kinase-mediated signaling, the role of PTPs is now recognized in initiating, sustaining, and terminating cellular signaling.[2,3] A comparison of PTP domains across diverse organisms suggests extensive sequence conservation and a conserved catalytic mechanism.[4] The involvement of PTP homologues in similar biological processes in both vertebrates and invertebrates emphasizes the evolutionary relationship of the PTP domains.[5] PTPs are broadly divided into two classes: ones anchored to the membrane by transmembrane helices, known as receptor protein tyrosine phosphatases (RPTPs), and cytosolic PTPs. RPTPs are further divided into subclasses on the basis of their extracellular domain arrangement.[4]

Drosophila melanogaster has approximately half the number of PTPs as either humans or the worm. These observations suggest that the fruit fly uses an optimal set of PTPs in consortia, in related pathways.[6] Genetic studies reveal that five RPTPs of *D. melanogaster* are expressed exclusively in the central nervous system (CNS) of the embryo. While four of these RPTPs (PTP10D, DLAR, PTP69D, and PTP99A) are expressed on CNS axons, PTP52F is present on both CNS axons and cell bodies.[7−9] The crucial role of PTP10D and PTP69D in regulating the repulsion of growth cones from the embryonic midline has been extensively studied.[10] More recently, behavioral and genetic experiments on memory formation in *D. melanogaster* reveal that PTP10D deletion mutants are chronically impaired in long-term memory.[11]

The dephosphorylation catalyzed by PTPs primarily depends on their active site cysteine residue located in the phosphate binding loop (P loop). The backbone dipoles of the P loop and the side chain dipole of the conserved serine in the P loop lower the pK_a of the active site cysteine.[12] This cysteine is thus retained in its thiolate (deprotonated) form and functions as a nucleophile to attack the phosphate of the incoming phosphotyrosine residue. Subsequently, the general acid aspartate of the WPD loop protonates the leaving group following substrate binding, resulting in the formation of a cysteinyl-phosphate enzyme−substrate intermediate. The intermediate is then hydrolyzed by the addition of a water molecule to release the active enzyme and the inorganic phosphate. This addition of water is facilitated by two glutamine residues of the Q loop.[13] While conserved residues of the P loop, WPD loop, and Q loop

Received: July 14, 2011
Revised: October 15, 2011
Published: October 18, 2011

have been extensively studied,[14] the role of residues in the substrate recognition loop that form the boundary of the PTP active site has received much less attention.

An ~9 Å deep cleft at the active site distinguishes a PTP from a dual-specificity phosphatase (~6 Å deep cleft). While the overall mechanism of dephosphorylation is the same in both PTP and dual-specificity phosphatases, a much deeper active site selects for a phosphotyrosine as opposed to a phosphothreonine or phosphoserine residue.[14] The boundary of this cleft is marked by an aromatic residue of the substrate recognition loop. The crystal structure of the PTP domain of *D. melanogaster* PTP10D in both native and phosphopeptide substrate (GP4)-bound forms provides an insight into the role of this residue in substrate recruitment. Two other complexes, with the inhibitors vanadate and *p*-nitrocatechol sulfate (PNC), provide a conformational basis for PTP activity. These structures provide the first evidence of the role of an aromatic residue in the substrate recognition loop in localizing the phosphotyrosine residue. In PTP10D, the aromatic ring of Phe76 stacks with the incoming substrate, thus facilitating substrate recruitment. This forms the first step for the insertion of a phosphotyrosine residue into the active site cleft of a PTP domain to interact with the nucleophilic cysteine at its base. We note that mutation of Phe76 to Leu results in an ~60-fold decrease in the catalytic efficiency of the enzyme. The mean lifetime of the phosphatase reaction is doubled, while the half-time of formation of the enzyme−substrate and/or enzyme−inhibitor complex is increased by 3-fold. Altogether, the crystal structures, enzymatic assays, and fluorescence measurements of inhibitor binding provide a conformational rationale for the role of the substrate recognition loop in mediating formation of the enzyme−substrate complex in this class of enzymes.

EXPERIMENTAL PROCEDURES

Cloning, Expression, and Purification of the PTP Domain of PTP10D. The cDNA cosmids for amplifying PTP10D via polymerase chain reaction (PCR) were obtained from K. Zinn (California Institute of Technology, Pasadena, CA). The DNA fragment encoding the catalytic domain of PTP10D (Arg1226−Asn1533) was cloned between the *Nhe*I and *Not*I sites of *Escherichia coli* expression vector pET28a. The forward and reverse primers were 5′-ATATGCTAGCCGCCCC-ATTCTGATCAAGAACTTTGCC-3′ and 5′-AATAATGCGGC-CGCCTAGTTCTCCTTCCCCTCGAGCACCGC-3′, respectively. A stop codon was incorporated in the reverse primer so that the recombinant protein harbored only the N-terminal polyhistidine tag. The plasmid containing the recombinant PTP domain was transformed into BL21(DE3) cells (Novagen, Inc.). The cells were grown to an optical density of 0.6 at 37 °C, whereupon the cells were induced with 0.3 mM isopropyl β-D-galactopyranoside (final concentration). Following this, the temperature for growth was lowered to 15 °C and cells were grown for 10−12 h before they were spun down. The cells were resuspended in lysis buffer (buffer L) containing 50 mM Tris-HCl (pH 8.0), 300 mM NaCl, 5% glycerol, and 1 mM β-mercaptoethanol (βME). After sonication on ice, the cell debris was separated from the crude cell lysate by centrifugation for 30 min at 15000 rpm in a centrifuge. The cell-free lysate was incubated with Ni-NTA affinity resin (approximately 4 mL of resin was used for cell-free lysate from 10 g of cell paste) at 4 °C for 2 h in an end-to-end rotor. The resin was then packed into a XK16 column (Amersham Biosciences) and washed with ~3 bed volumes of a buffer containing 50 mM Tris-HCl (pH 8.0), 7 mM imidazole, 300 mM NaCl, 5% glycerol, and 1 mM βME. The protein was eluted with a gradient of imidazole (7 to 200 mM) prepared in buffer L. The pure fractions were pooled and concentrated using a centricon (Millipore) and loaded onto an S200 size exclusion column (Amersham). The protein was eluted in 30 mM Tris-HCl (pH 7.5), 300 mM NaCl, and 5% glycerol. The peak fractions were pooled, concentrated, and used for crystallization and biochemical studies.

Site-Directed Mutagenesis. The catalytic domain of PTP10D was modified to yield single-mutant (F76L, D210A, and C242S) and double-mutant (D210A/Q286A and C242S/Q286A) proteins. While the D210A, C242S, and Q286A mutations were at the active site of the PTP domain, the F76L mutation was in the phosphotyrosine recognition loop. A single-primer approach was used for site-directed mutagenesis, with an overlap of 10 nucleotides on either side of the mutation. Unique restriction sites were incorporated in the primer to aid screening of mutants. After PCR (Phusion Polymerase, Finnzymes), the parent template was digested with *Dpn*I at 37 °C and the mutated template was transformed in DH5α cells. All mutants were confirmed by sequencing (Macrogen Inc.).

Substrates and Inhibitors for Structural and Biochemical Analysis. Peptide sequences corresponding to the SH2 interacting regions of glycoprotein GP150 that was previously shown to be a substrate for PTP10D in *Drosophila* S2 cells were designed.[15] The sequence of GP150 was obtained from the nonredundant protein database at the National Center for Biotechnology Information. Four peptides incorporating one phosphotyrosine residue each from the four immunoreceptor family tyrosine-based activation motifs (ITAM) in the cytosolic tail of GP150 were designed. The following peptide sequences were used: GP1, KRGERpYRMALL; GP2, LMRVI-pYWLRKR; GP3, PKVHRpYAPINQ; and GP4, KNSFVpYQKLSE. All four peptides in their phosphorylated form were obtained commercially at >99% purity from GL Bioscience. The physicochemical properties of the peptides were estimated from the peptide calculator at the Novagen custom peptide Website (http://www.innovagen.se/custom-peptide-synthesis/peptide-property-calculator/). The small molecule substrate *p*-nitrophenyl phosphate (*p*NPP) and the inhibitors *p*-nitrocatechol sulfate (PNC) and sodium vanadate were obtained from Sigma Aldrich, Inc.

Crystallization and Structure Determination. Purified PTP10D (10 mg/mL) was screened for crystallization conditions using commercially available screens. Crystals were observed under several conditions that included small chain alcohols and PEG 3350. Optimal crystals were obtained in crystallization drops containing 3 μL of ~7 mg/mL protein and 3 μL of a solution containing 120 mM citrate, 15% PEG 4000, 10% 2-propanol, 10% *n*-butanol, and 10% 1,4-butanediol. These crystals appeared within 10 days in microbatch trials using a 2:1 ratio of Paraffin to silicon oil (Hampton Research). Crystals were flash-frozen in a cryoprotectant containing 5% PEG 400 under the crystallization conditions. Inclusion of 5 mM tris(2-carboxyethyl)phosphine (TCEP) in the cryoprotectant was crucial for obtaining an isotropic diffraction pattern. The diffraction data sets corresponding to the substrate and inhibitor complexes were obtained for crystals soaked in 0.8 mM phosphopeptides GP1−GP4 (substrate peptide) and 5 mM PNC or 5 mM sodium vanadate for the inhibitor complexes.

X-ray diffraction data was collected on beamline BM14 of the European Synchrotron Radiation Facility (Grenoble, France).

Diffraction images were processed using MOSFLM[16] and scaled using SCALA.[17] Phase information was obtained by molecular replacement, performed using PHASER[18,19] with the crystal structure of the catalytic domain of human tyrosine receptor phosphatase β [Protein Data Bank (PDB) entry 2AHS, 55% identical] as the search model. The molecular replacement utility CHAINSAW[20] was used to modify the model structure by pruning nonconserved residues. The structures of the complexes were determined by using native PTP10D as the search model. Structures were refined using REFMAC5,[21] and the fit of the model to the electron density was evaluated using COOT.[22] The topology and parameter files for various ligands were obtained from the PRODRG server.[23] Models were validated using MolProbity[24] and the WHATIF server.[25] Interatomic distances were calculated using CONTACT from the CCP4 suite.[26]

In silico mutation of Phe76 to Leu was performed on the WHATIF server.[25] Neuronal network combinations at the HotPatch server[27] were used to identify residues lining the active site of the catalytic domain of PTP10D. All protein structural representations were made using PyMOL (DeLano Scientific). The sequences of individual PTP domains were obtained from the PTP database.[4] Multiple-sequence alignment and the percentage occurrence of the amino acid were calculated with Jalview.[28]

Circular Dichroism and Steady State Fluorescence Measurements. Secondary structure and tertiary structure changes upon mutagenesis in PTP10D were ascertained by circular dichroism (CD) and intrinsic tryptophan fluorescence measurements. CD measurements were recorded at a protein concentration of 1 μM on a Jasco-J715A spectropolarimeter using a 0.1 cm path-length cuvette. Spectra were recorded with a slit width of 1 nm and a response time of 4 s at a scan rate of 50 nm/min. Fluorescence emission spectra were recorded on a Jasco SPEX Fluoromax-3 instrument using a 1 cm cuvette. Samples were excited at 280 nm, and spectra were recorded from 300 to 400 nm. Each data point was an average of three scans. The excitation and emission slit widths were maintained at 3.5 and 5 nm, respectively. For all spectral measurements, the buffer consisted of 25 mM HEPES (pH 7.0), 150 mM NaCl, and 2 mM DTT.

Phosphatase Assays and Time Course Measurements. Phosphatase assays using *p*NPP as the substrate were performed as described previously[29] in buffer A [50 mM citrate, glycine, and HEPES (CGH) (pH 6.5), 100 mM NaCl, and 2 mM DTT]. Phosphatase activity with the phosphotyrosine-containing peptides was ascertained by the detection of inorganic phosphate released by the malachite green reaction.[30] Phosphopeptide stocks were prepared in 50 mM citrate (pH 6.5) and 100 mM NaCl. Peptide concentrations were estimated by measuring the absorbance at 268 nm. Increasing concentrations of peptides were incubated with 0.125 μM PTP10D (0.5 μM F76L mutant) in buffer B [25 mM citrate buffer (pH 6.5), 2% glycerol, 150 mM NaCl, and 2 mM DTT] at 25 °C for 15 min. The reaction was stopped by the addition of 5 times the reaction volume of Biomol Green reagent (Enzo Life Sciences). The amount of inorganic phosphate released was estimated by measuring the absorbance at 650 nm. For all assays, kinetic constants for steady state catalysis were obtained by fitting the reaction curves to the Michaelis–Menten equation using the nonlinear regression module of SigmaPlot (Systat Software, Inc.).

For time course measurements, dephosphorylation was initiated by addition of 0.5 μg of PTP10D to 35 mM *p*NPP in buffer A. Formation of *p*-nitrophenol (*p*NP) was monitored at 405 nm in continuous mode (every 0.5 s) for 25 min. For time course measurements with peptides, 0.5 μg of protein was incubated with peptides at concentrations 5 times their K_m values (Table 2) in reaction buffer B. An aliquot was taken from the main reaction mixture and the reaction stopped by the addition of Biomol Green reagent every 2 min for 25 min. As the time course measurements were performed at saturating substrate concentrations, the rate of product formation was fitted to a pseudo-first-order reaction (dependent only on the concentration of the ES complex) using the equation

$$v = \alpha(1 - e^{-\lambda t}) \quad (1)$$

where v is the reaction velocity (nanomoles of product per minute), t is time (minutes), α is the maximum amount of product formed at the end of the time course, and λ is the rate of the increase in reaction velocity to its maximum and is related to the $t_{1/2}$ of the reaction as

$$t_{1/2} = \ln(2)/\lambda \quad (2)$$

The mean lifetime of the reaction is defined as

$$\tau = 1/\lambda \quad (3)$$

Inhibitor Binding Studies. The inhibition constant (K_i) was estimated using protocols reported previously.[31] Sodium vanadate (1 mM) was prepared in water, and concentrations of subsequent dilutions were estimated by the absorbance at 260 nm (ε^M = 3550 M^{-1} cm^{-1}). Steady state Michaelis–Menten kinetics for *p*NPP were monitored in the presence of 0.2, 0.5, 0.75, 1.0, and 2.5 μM sodium vanadate in reaction buffer A at 25 °C. The data were simultaneously fit to nonlinear regression equations for competitive inhibitor binding by the GraphPad Prism (GraphPad). A Dixon plot was plotted for increasing concentrations of vanadate and the reciprocal of reaction velocities to obtain a set of intersecting lines that provide an independent estimate of inhibition constant K_i.

PNC binding was monitored using the intrinsic tryptophan quenching of the WPD loop of the PTP domain upon inhibitor binding.[32] PTP10D (5.0 μM) and its single and double mutants were incubated with increasing concentrations of PNC (from 0 to 1.2 mM) in buffer B for 15 min at 25 °C. Fluorescence measurements were performed on a Jasco SPEX Fluoromax-3 instrument using a 1 cm cuvette. Excitation and emission wavelengths were fixed at 280 and 360 nm, respectively. The slit widths for the excitation and emission monochromators were fixed at 3.5 and 5.0 nm, respectively. All measurements were an average of five readings with an integration time of 0.2 s.

PNC binding kinetics were monitored on a Jasco FP-6300 spectrofluorometer in a 1 cm cuvette to minimize the dead time of the reaction. The reaction was initiated via addition of 600 μM PNC to 1.5 μM protein. Fluorescence quenching was monitored in real time at 360 nm upon excitation at 280 nm for 300 s (response time of 0.1 s). A slit width of 3.0 nm was used for both the excitation and emission monochromators.

The fraction of protein bound to PNC was estimated using

$$f_{(x)} = [Y_{(x)} - Y_{unbound}]/(Y_{bound} - Y_{unbound}) \quad (4)$$

where $Y_{(x)}$ is the fluorescence signal of the protein at a PNC concentration of x, $Y_{unbound}$ is the fluorescence signal of the

Table 1. Data Collection, Refinement, and Model Statistics for Apo and Ligand-Bound PTP10D Structures

	PTP10D	PTP10D with GP4	PTP10D with vanadate	PTP10D with PNC
PDB entry	3S3E	3S3H	3S3F	3S3K
		Data Collection[a]		
wavelength (Å)	0.954	1	1	1
space group	$P3_121$	$P3_121$	$P3_121$	$P3_121$
cell dimensions	a = 102.45 Å	a = 102.70 Å	a = 103.07 Å	a = 102.51 Å
	b = 102.45 Å	b = 102.70 Å	b = 103.07 Å	b = 102.51 Å
	c = 171.81 Å	c = 173.22 Å	c = 173.40 Å	c = 172.80 Å
resolution limits (Å)	44.0−2.40 (2.53−2.40)	45.0−2.80 (2.95−2.80)	45.0−2.70 (2.85−2.7)	45.0−3.20 (3.37−3.20)
R_{merge}[b] (%)	11.9 (48.4)	11.4 (45.6)	11.3 (43.5)	16.4 (42.6)
$(I)/\sigma(I)$	15.9 (5.2)	10.6 (3.1)	11.9 (3.7)	4.7 (2.4)
no. of unique reflections	41551 (5989)	26708 (3832)	29943 (4297)	17564 (2523)
completeness	100.0 (100.0)	100.0 (100.0)	100.0 (100.0)	98.7 (99.0)
multiplicity	11.2 (11.3)	5.3 (5.4)	5.8 (5.8)	3.1 (3.1)
average mosaicity	0.41	0.66	0.57	0.67
		Refinement		
R_{cryst}[c] (%)	20.45	25.01	23.81	25.29
R_{free} (%)	22.72	28.92	27.18	30.86
		Model		
Ramachandran Plot				
Preferred	538 (94.72%)	532 (93.66%)	540 (95.07%)	514 (90.49%)
Allowed	26 (4.58%)	31 (5.46%)	24 (4.23%)	47 (8.27%)
Outliers	4 (0.70%)	5 (0.88%)	4 (0.70%)	7 (1.23%)
rmsd for bond lengths (Å)	0.007	0.011	0.009	0.008
rmsd for bond angles (deg)	1.178	1.401	1.261	1.194
Wilson B (Å^2)	38.12	54.12	44.99	56.63
mean B (Å^2)	27.75	49.60	38.07	54.07

[a]Values in parentheses are for the outer resolution shell. [b]$R_{merge} = \sum_j|\langle I\rangle - I_j|/\sum\langle I\rangle$, where I_j is the intensity of the jth reflection and $\langle I\rangle$ is the average intensity. [c]$R_{cryst} = \sum|F_o - F_c|/\sum|F_o|$; R_{free} is the same as R_{cryst} but for 5% of the data excluded from the refinement calculation.

protein in the absence of PNC, and Y_{bound} is the fluorescence signal of the protein at a saturating concentration of PNC. The graph was then fitted to a conventional ligand binding nonlinear regression equation using SigmaPlot.

The following equation was used to fit the kinetic data:

$$V = v_o + \alpha/[1 + e^{-\beta(t-t_{1/2})}] \quad (5)$$

where V is the rate of PNC binding, v_o is the unbound baseline correction, α is the maximum difference in the fluorescence signal of the bound and unbound protein, β describes the slope of the curve, and $t_{1/2}$ is half-time of PNC binding defined by the first-derivative maximum of the sigmoid function. t_o was used to define the lag phase of the curve. All equations were fit to experimental data using the nonlinear regression module of SigmaPlot.

RESULTS

Structure of the Catalytic Domain of PTP10D and Substrate Complexes. The catalytic domain of PTP10D and its active site mutants were purified to homogeneity. Circular dichroism (CD) and fluorescence spectra of the recombinant proteins suggest that the mutations do not alter the overall structure of PTP10D. A modification of the recombinant protein construct incorporating an additional 47 residues at the N-terminus of the classical PTP domain was crucial for obtaining protein samples at the concentration required for crystallization. As reported previously, despite poor sequence similarity in the N-terminal segment (preceding the M1 PTP motif), this polypeptide stretch adopts an α-helical conformation and contributes to the stability of the PTP domain, a feature seen both in PTP10D and in few other structures where this segment has been included in the PTP domain construct [for example, RPTPα (PDB entry 1YFO)].[29] The native PTP10D and the PTP10D active site mutant proteins are monomers in solution (Figure S1 of the Supporting Information).

This catalytic domain of PTP10D crystallized in space group $P3_121$ with two molecules in the asymmetric unit. Molecular replacement using the catalytic domain of PTP-β yielded a single solution with a log likelihood gain (LLG) of 2886. The data, refinement, and model statistics are compiled in Table 1. For ease in comparison with other characterized PTP domains, residues in the catalytic domain of PTP10D were numbered from 1 to 305 (Figure 1 and Figure S1 of the Supporting Information). PTP10D adopts the classical PTP fold with a central twisted β-sheet composed of eight β-strands (Figure 1). This β-sheet is flanked by eight α-helices, two of which form the N-terminal helix−turn−helix motif crucial for protein solubility and stability.[29] The P loop located between β8 and α4 contains the nucleophilic cysteine (Cys242 in PTP10D) and forms the base of the active site. This cysteine is flanked by the general acid/base aspartate (Asp210) from the WPD loop (located between β7 and α3) and the glutamines (residues 286 and 290) of the Q loop (between α5 and α6). A structure-based sequence analysis revealed that the 10 PTP motifs (reviewed in ref 4) are conserved in PTP10D (Table 1 and Figures S3 and S4 of the Supporting Information). The

dx.doi.org/10.1021/bi201092q|Biochemistry 2011, 50, 10114−10125

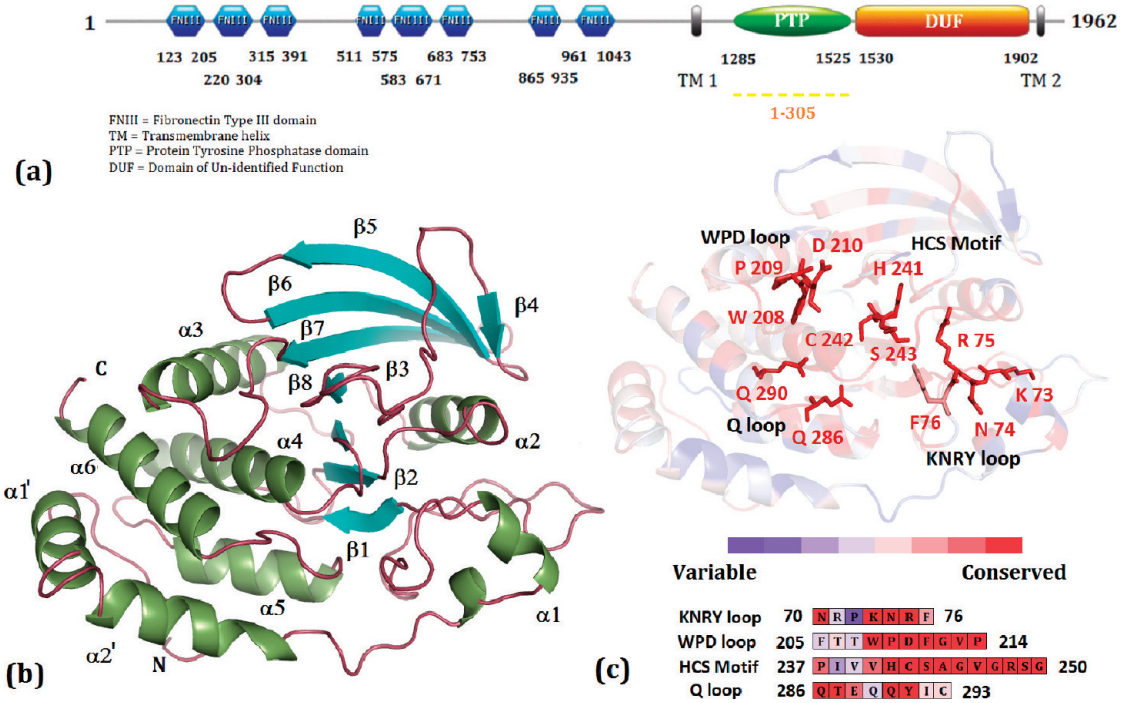

Figure 1. Sequence and structural features of the catalytic domain of PTP10D. (a) Domain organization of *D. melanogaster* PTP10D. The sequence of the catalytic domain has been renumbered from 1 to 305 to facilitate comparisons with other PTP domains. (b) Catalytic domain of PTP10D. (c) PTP sequence motifs mapped onto the structure of PTP10D.

structure of PTP10D with the phosphopeptide substrate GP4 and the inhibitors vanadate and PNC showed clear electron density for the ligand at the active site of one monomer (chain B) of the two in the asymmetric unit. This observation is consistent with crystal packing that reveals that the active site of chain B is more accessible to the solvent (Figure S2 of the Supporting Information). An analysis of the PTP10D structure and the ligand complexes using Molprobity[24] revealed that a few residues in these structures were outliers in the Ramachandran plot. A prominent outlier is the active site cysteine (Cys242). Other outliers include residues in the loop adjacent to the active site. This loop segment changes conformation upon ligand binding. An inspection of the fit of the model to the electron density as well as high real space correlation coefficients (~0.8−0.9) suggests that these residues have been correctly modeled in these crystal structures.

Conformational Features of the Active Site. Superposition of the ligand-bound and apo structures of PTP10D with the "closed" conformation of PTP1B (PDB entry 1SUG) reveals that all PTP10D structures adopt the "open" conformation of the active site loop (Figure 2 and Figure S5 of the Supporting Information). This superposition suggests that the hinge prolines (Pro209 and Pro214 in PTP10D) retain the WPD loop in the open conformation. The general acid, Asp210, in PTP10D is 13.8 Å from the active site Cys242 as opposed to the equivalent Asp181 in PTP1B, which is 8.8 Å from Cys215. The difference in the orientation of the side chain of Phe211 is the most distinct between the bound and free PTP10D structures.

The water molecule network at the active site of the PTPs has been described previously. In general, two ordered water molecules and one disordered water molecule are seen in the active site of PTPs.[33] In PTP10D, all three water molecules could be unambiguously modeled with *B* factors of 12.64, 18.97, and 21.05 Å^2 for waters W1−W3, respectively (Figure 3a and Figures S6 and S7 of the Supporting Information). While W1 is coordinated by Cys242 and Gln286, and W2 is bound by Cys242 and Lys154. W3 is loosely associated with Cys242 and Gln286 and represents the disordered water at the PTP active site. Ligand binding at the PTP active site requires sequential removal of these water molecules as noted from the structures of the enzyme−substrate and enzyme−inhibitor complexes of PTP10D.

PTP10D crystals incubated with the phosphopeptide GP4 showed unambiguous electron density at the active site that could be attributed to a phosphotyrosine residue. The electron density for the rest of the bound peptide was poor; the flanking segments were thus not modeled in this crystal structure (2.8 Å resolution). The bound phosphotyrosine, however, reveals several facets of substrate recognition. The phenyl ring of this residue makes planar stacking interactions with Phe76 (aromatic ring stacking distance of 4.5 Å) such that the phosphate of the phosphotyrosine is aligned with the nucleophilic Cys242. The phosphotyrosine also displaces one of the water molecules (W3) that is most loosely associated in the active site. Waters W1 and W2 could be modeled at the active site with the side chain of Lys154 coming closer to W2 by 0.3 Å. The carboxyl and amino termini of the phosphotyrosine residue make hydrogen bonds with Gln286 and Asn78 that regulate access to the PTP10D active site (Figure 3b).

p-Nitrocatechol sulfate (PNC), a competitive inhibitor of PTPs, mimics phosphotyrosine.[34] In the structure of the PTP10D−PNC complex, one PNC molecule could be modeled into the active site. As in the substrate peptide complex, Phe76 makes planar stacking interactions with the PNC molecule. However, this molecule is located deeper in the active site of PTP10D than the phosphotyrosine of the peptide substrate

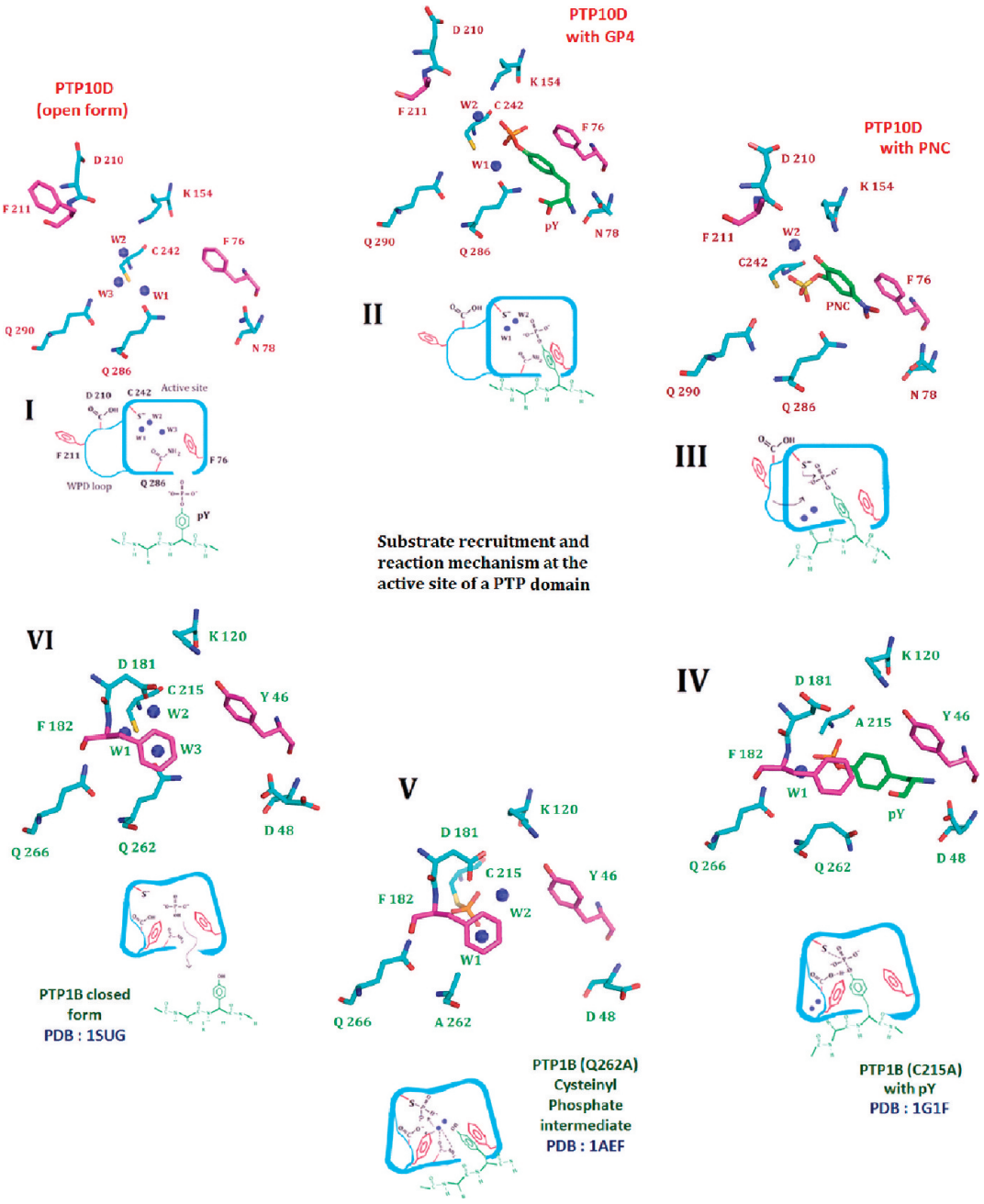

Figure 2. Crystal structure of PTP10D that offers mechanistic insights into distinct steps of the phosphatase reaction. (I) The deprotonated active site cysteine prior to entry of the substrate into the active site. Three conserved water molecules hydrate the active site of PTP10D (PTP10D open structure). (II) Entry of the substrate into the active site is mediated by Phe76 of the KNRY loop (based on the structure of PTP10D with the GP4 peptide). The incoming substrate displaces water W3. (III) The substrate approaches the active site cysteine by displacing water W1. Aryl stacking interactions with Phe76 maintain the optimal conformation of the incoming substrate (based on the crystal structure of PTP10D with PNC). (IV) The WPD loop closes for the conserved active site phenylalanine (Phe182) to make stacking interactions with the substrate. The conformation of the substrate is optimized to aid catalysis. This orientation is perpendicular to that noted in step II (based on the PTP1B−phosphotyrosine complex). (V) The optimized orientation of the substrate ensures catalysis. The cysteinyl−phosphate intermediate as seen in the active site of PTP1B. (VI) The cysteinyl−phosphate intermediate is hydrolyzed by addition of water by glutamines of the Q loop. The active site cysteine reverts to its free, deprotonated state with three waters at the active site (based on the PTP1B closed form structure).

(Figure 3c). We also note that the sulfate of the PNC molecule displaces water W1. This position of the sulfate is the same as that of the phosphate of the phosphotyrosine seen in PTP−substrate structures reported previously.[35,36] In this study, sodium vanadate was also used as an inhibitor as it adopts an inorganic phosphate-like geometry as well as a five-coordinate trigonal bipyramidal structure that resembles the transition state of the phosphotransfer reaction.[37] Crystals soaked in vanadate showed a tetrahedral electron density in chain B that could be attributed to vanadate (Figure 3d). We note that vanadate binding displaces the waters at the active site.

Phosphatase Activity and Time Course Measurements for PTP10D and the F76L Mutant. The phosphatase activity measured using either *p*NPP or phosphopeptide

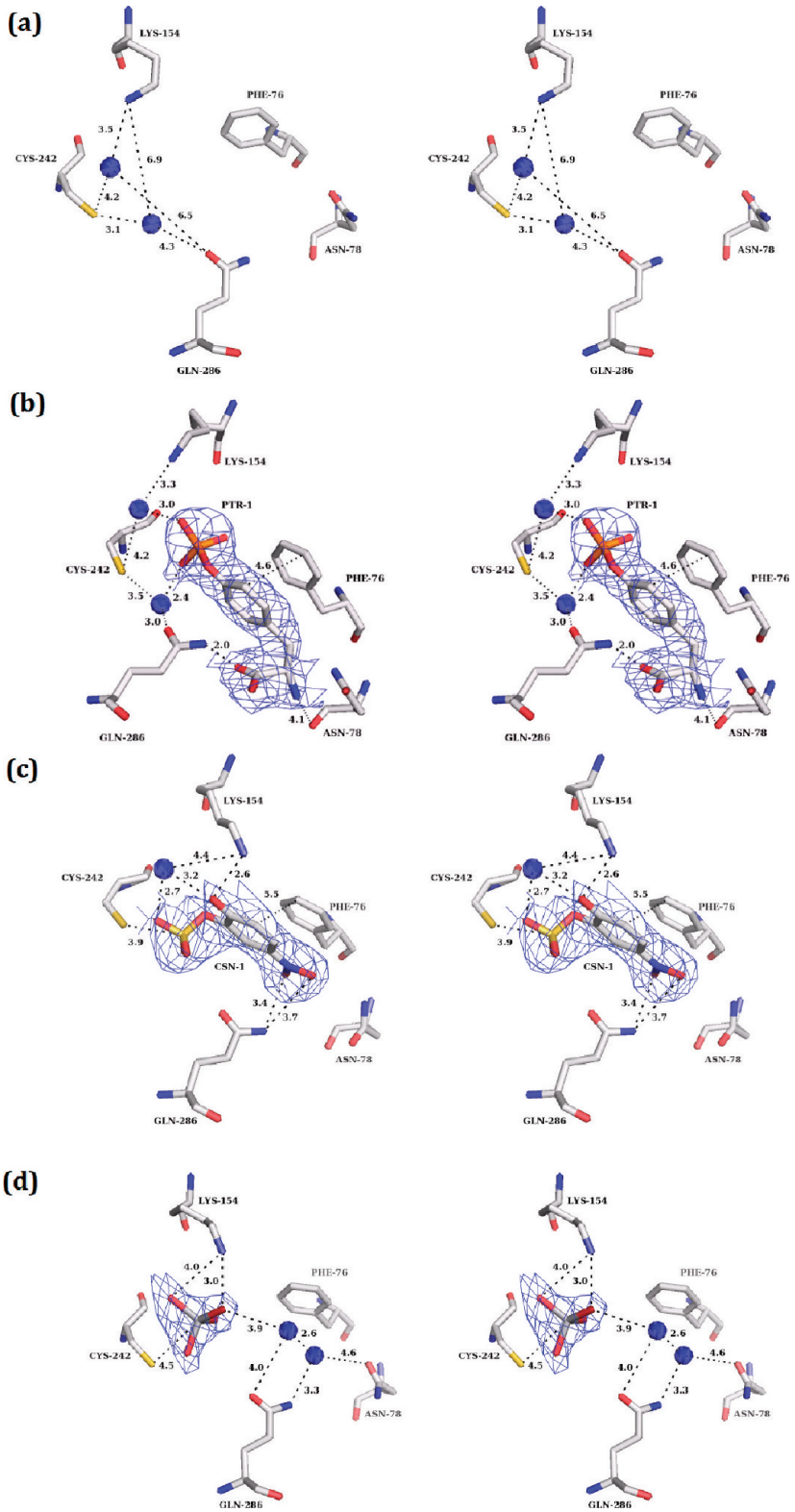

Figure 3. Apo and substrate/inhibitor-bound active site of PTP10D. $mF_o - DF_c$ electron density maps (at 3.0σ) for the apo and substrate/inhibitor-bound states of PTP10D: (a) active site of apo PTP10D (PDB entry 3S3E, 2.4 Å resolution), (b) phosphotyrosine of the GP4 peptide at the active site of PTP10D (PDB entry 3S3H, 2.8 Å resolution), (c) PNC bound at the active site of PTP10D (PDB entry 3S3K, 3.2 Å resolution), and (d) vanadate bound at the active site of PTP10D (PDB entry 3S3F, 2.7 Å resolution).

substrates reveals PTP10D to be a highly efficient enzyme. PTP10D could dephosphorylate all four GP150 immunoreceptor family tyrosine-based activation motif (ITAM) peptide substrates. While the catalytic efficiency was highest in the case of peptides harboring charged groups around the central phosphotyrosine (GP1 and GP3), the affinity of PTP10D was maximal for a peptide having small chain residues adjacent to the phosphotyrosine (GP4). The dephosphorylation catalyzed

Table 2. Enzyme Kinetic Parameters for PTP10D and the F76L Mutant Determined Using Different Substrates

	V_{max} (μmol min^{-1} mg^{-1})	K_m (μM)	k_{cat} (s^{-1})	k_{cat}/K_m ($\times 10^3$ s^{-1} M^{-1})
		PTP10D		
*p*NPP	13.74 ± 1.40	5312.80 ± 58.42	8.24 ± 0.89	1.55 ± 0.16
GP1	10.45 ± 0.48	138.05 ± 6.43	6.65 ± 0.32	48.18 ± 2.39
GP2	6.24 ± 0.55	508.11 ± 45.21	3.92 ± 0.34	7.71 ± 0.67
GP3	10.33 ± 0.41	129.67 ± 5.07	6.47 ± 0.26	50.15 ± 2.11
GP4	6.82 ± 0.24	69.88 ± 2.24	4.27 ± 0.15	61.11 ± 2.14
		PTP10D F76L Mutant		
*p*NPP	8.01 ± 0.84	24891.9 ± 387.09	4.80 ± 0.50	0.19 ± 0.02
GP1	3.33 ± 0.39	1081.24 ± 133.17	2.00 ± 0.24	1.85 ± 0.22
GP2	0.83 ± 0.11	2564.83 ± 355.26	0.52 ± 0.07	0.21 ± 0.03
GP3	3.54 ± 0.46	1009.29 ± 137.87	2.12 ± 0.27	2.11 ± 0.27
GP4	1.49 ± 0.13	542.95 ± 48.67	0.89 ± 0.08	1.64 ± 0.15

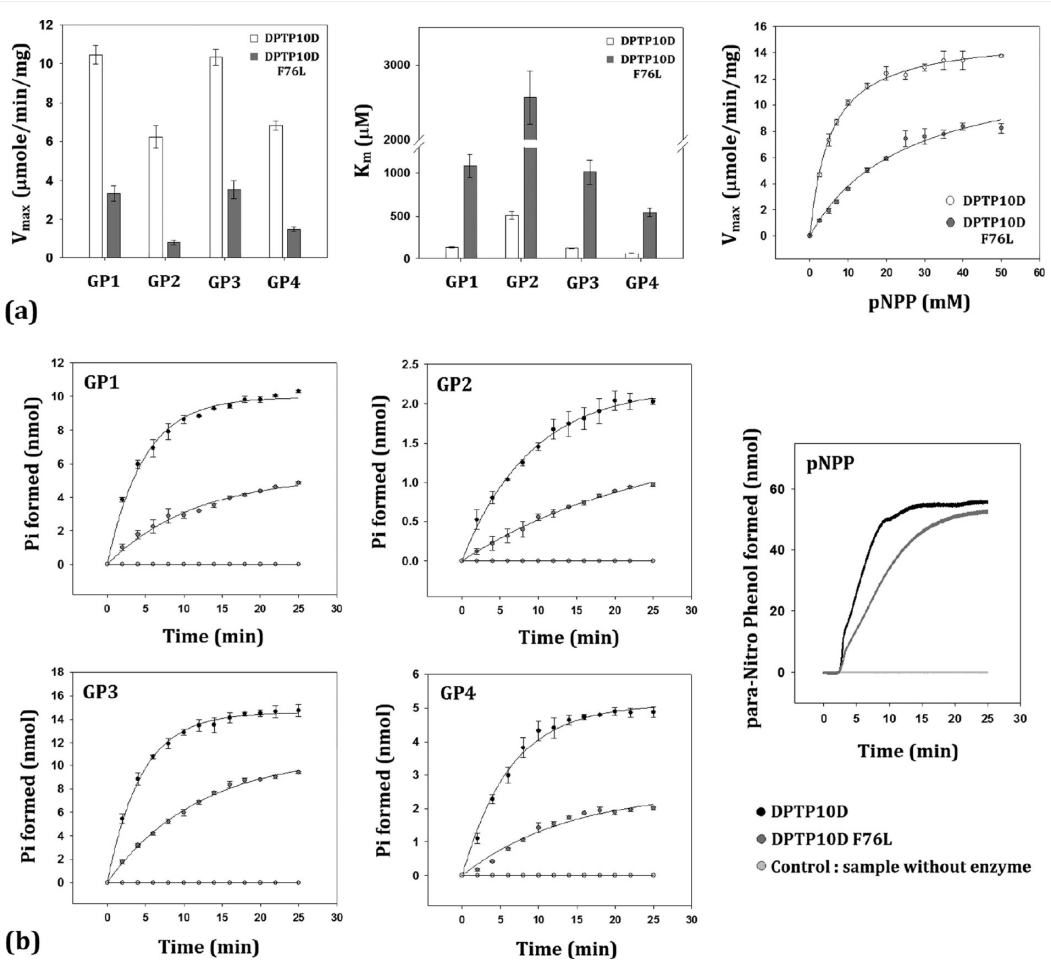

Figure 4. Phosphatase assays and time course measurements for PTP10D. (a) Michealis–Menten kinetics for the phosphatase activity of PTP10D and the F76L mutant with various substrates. (b) Time course measurements to ascertain the lifetime of the phosphatase reaction as catalyzed by PTP10D and the F76L mutant.

by PTP10D was least efficient for GP2, which harbored nonpolar and aromatic residues around the phosphotyrosine. This suggested that substrate recognition is largely influenced by charges on the surface and the size of the side chains (Table 2 and Figure 4). Mutation of Phe76 to Leu led to a 7-fold decrease in the V_{max} for all substrates of PTP10D and an 8-fold increase in the K_m values. While this mutation decreased the overall efficiency of PTP10D, it did not alter substrate preference characteristics. Time course measurements reveal that the mean lifetime (τ) as well as the $t_{1/2}$ of the phosphatase reaction increased by more than 2-fold in the F76L mutant compared to those of native PTP10D (Table 3 and Figure 4). The amount of product formed at the end of the time course for the F76L is smaller by a factor of ~0.45 when compared to the amount of the native protein. This observation is consistent with the decrease in the V_{max} of the phosphatase reaction and is also reflected in the decrease in the overall rate of the pseudo-first-order reaction (λ).

dx.doi.org/10.1021/bi201092q | *Biochemistry* 2011, 50, 10114–10125

Table 3. Parameters for the Phosphatase Reaction Catalyzed by PTP10D and the F76L Mutant

	PTP10D				PTP10D F76L			
	α (nmol)	λ ($\times 10^{-2}$ min^{-1})	τ (min)	$t_{1/2}$ (min)	α (nmol)	λ ($\times 10^{-2}$min^{-1})	τ (min)	$t_{1/2}$ (min)
*p*NPP	55.77 ± 1.12	16.43 ± 0.32	6.08 ± 0.12	4.22 ± 0.08	52.80 ± 0.79	6.12 ± 0.92	16.34 ± 0.25	11.32 ± 0.17
GP1	9.96 ± 0.49	20.99 ± 1.06	4.76 ± 0.24	3.30 ± 0.17	5.36 ± 0.56	8.51 ± 0.84	11.74 ± 1.15	8.13 ± 0.79
GP2	2.21 ± 0.14	11.07 ± 0.72	9.03 ± 0.59	6.26 ± 0.41	1.61 ± 0.17	3.89 ± 0.41	25.70 ± 2.69	17.81 ± 1.87
GP3	14.58 ± 0.37	22.26 ± 0.56	4.50 ± 0.11	3.11 ± 0.08	10.81 ± 0.65	8.39 ± 0.41	11.91 ± 0.59	8.26 ± 0.49
GP4	5.12 ± 0.32	15.76 ± 0.95	6.35 ± 0.41	4.39 ± 0.28	2.54 ± 0.24	7.18 ± 0.68	13.92 ± 1.32	9.65 ± 0.93

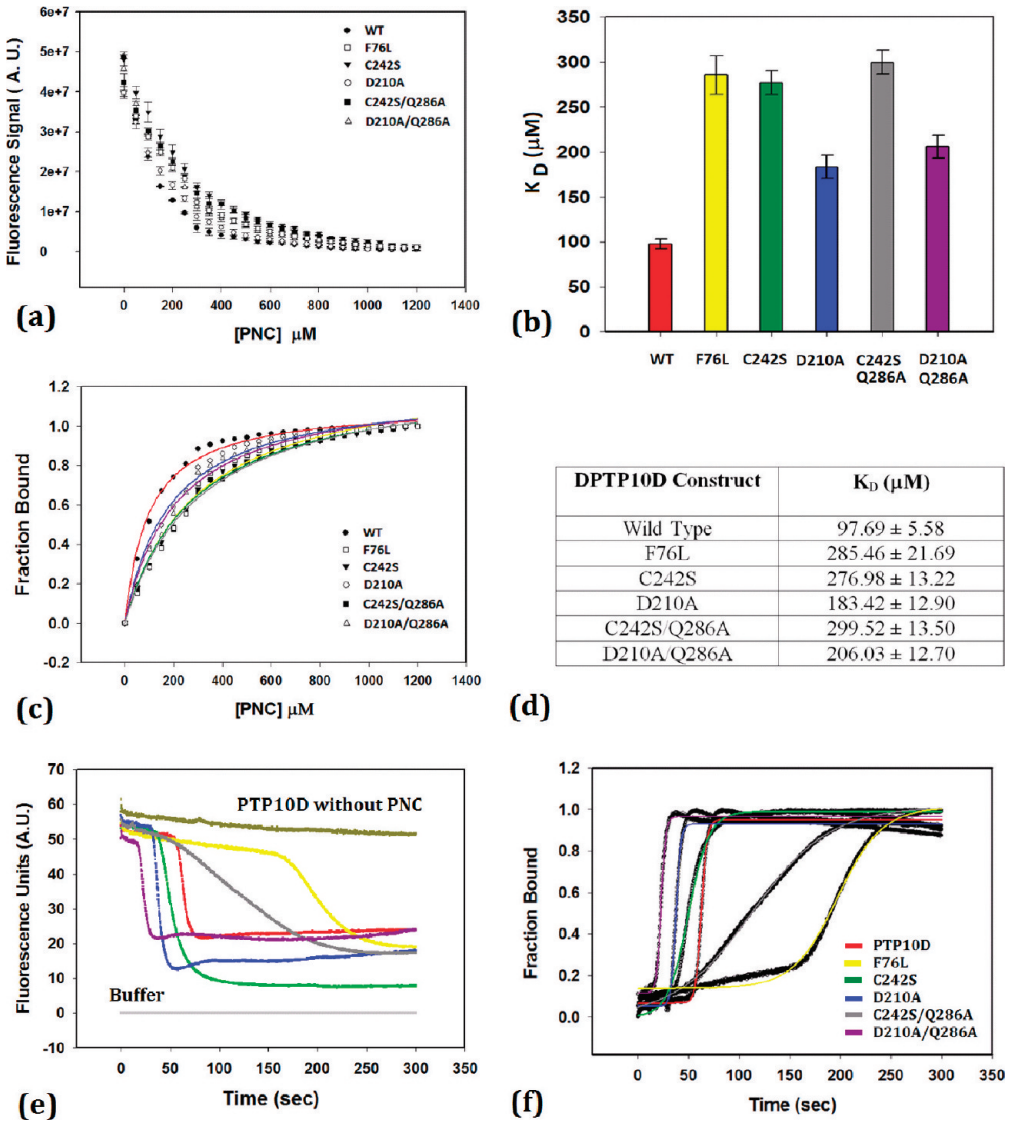

DPTP10D Construct	K_D (μM)
Wild Type	97.69 ± 5.58
F76L	285.46 ± 21.69
C242S	276.98 ± 13.22
D210A	183.42 ± 12.90
C242S/Q286A	299.52 ± 13.50
D210A/Q286A	206.03 ± 12.70

Figure 5. *p*-Nitrocatechol sulfate (PNC) binding to PTP10D and mutant enzymes. (a) Intrinsic tryptophan fluorescence quenching of PTP10D and its mutants upon PNC binding. (b and d) Dissociation constants for binding of PNC to PTP10D and its mutants. (c) Fraction of PTP10D bound to PNC to ascertain the ligand saturation. (e and f) Kinetics of association of PNC with PTP10D.

Addition of vanadate to the reaction mixture increased the K_m of the reaction but did not affect the V_{max} of the reaction. The enzyme inhibition constant (K_i) was found to be 1.53 ± 0.14 μM. The Michaelis−Menten and Dixon plots are shown in Figure S8 of the Supporting Information. This K_i value is 3 times higher than that for vanadate inhibition of PTP1B activity.[38] Steady state measurements to ascertain the dissociation constant of PNC binding (K_D) showed that mutations at the active site increase the K_D for PNC binding (Figure 5). As expected, a mutation of the active site Cys242 to serine caused a 3-fold decrease in the affinity for PNC, while that of the general acid/base Asp210 was less disruptive. Double mutations that serve as substrate trap mutants[39] also show weaker binding of PNC to PTP10D. The F76L mutation was seen to influence PNC binding as much as the C242S/Q286A mutant protein (Figure 5).

Kinetic measurements reveal that the lag time (t_o) for PNC binding is the longest (160 s) for the F76L mutant (Figure 5

dx.doi.org/10.1021/bi201092q|*Biochemistry* 2011, 50, 10114–10125

and Table 4) when compared to that of either wild-type PTP10D or the active site mutants. While mutations at the active site decreased the lag time for PNC binding (likely by altering the water network at the active site), the F76L mutation drastically increased the lag time for binding of PNC to PTP10D. An increase of ~130 s in the $t_{1/2}$ of PNC binding thus supports the role of Phe76 in mediating ligand entry at the PTP active site.

Table 4. Kinetic Parameters, Rate Constants, and Half-Lives of PNC Binding Obtained for PTP10D and Mutant Proteins

	t_o (s)	α (AU)	β ($\times 10^{-2}$ AU/s)	$t_{1/2}$ (s)
wild type	50.0	0.88 ± 0.01	35.97 ± 0.04	62.89 ± 0.04
F76L	160.0	0.87 ± 0.03	4.57 ± 0.01	197.22 ± 0.25
C242S	35.0	0.90 ± 0.01	12.51 ± 0.07	52.14 ± 0.08
D210A	30.0	0.87 ± 0.02	42.01 ± 0.05	37.73 ± 0.05
C242S/Q286A	40.0	1.04 ± 0.02	2.49 ± 0.03	111.07 ± 0.14
D210A/Q286A	16.0	0.85 ± 0.02	44.24 ± 0.04	22.9 ± 0.05

DISCUSSION

The structure of the PTP domain of a *D. melanogaster* RPTP (PTP10D), a protein implicated in memory and nervous system development, was determined in both apo and substrate-bound forms. An analysis of the surface of PTP10D by the HotPatch server suggests that the active site cleft is demarcated by residues Asn78, Phe76, Lys154, Gly247, Arg248, and Gln286 (Figure S5 of the Supporting Information). The entry of a substrate into the active site cleft is governed by residues Asn78 and Gln286. The nucleophilic Cys242 lies at the bottom of this cleft and is hydrated by three conserved water molecules. A close inspection of the native, phosphotyrosine-bound, and PNC-bound structures shows the protein backbone superposes well with an rmsd of <0.25 Å. Variations in the EKGERK, AEQR, and DDD loops in the ligand-bound and unbound forms of PTP10D provide insight into the conformational changes at the active site upon ligand binding (Figures S9 and S10 of the Supporting Information). Interactions between the active site and the WPD loop are mediated by the EKGERK loop. While glutamate (Glu149) makes bidentate salt bridges with Arg248 (connected to the AEQR loop) at the base of the active site, Lys150 makes a salt bridge with Asp210 of the WPD loop.

A comparison of the substrate peptide and PNC-bound structures of PTP10D with other PTP complexes[34,35] provides further insights into the mode of phosphotyrosine binding at the active site (Figure 2). The cavity of the active site of the PTP domain is constrained by Asn78 (Asp48 in PTP1B and Asp69 in YopH) and Gln286 (Gln262 in PTP1B and Gln284 in YopH) to specifically allow a phosphorylated tyrosine residue. Phe76 (equivalent to Tyr46 in PTP1B and Phe67 in YopH) forms the boundary of the active site and makes hydrophobic interactions with the phenyl ring of the incoming substrate. The structure reveals that Phe76 assists the substrate in adopting a conformation required to access the active site. The entry of the phosphotyrosine at the active site displaces water W3 that is loosely bound, thereby contacting the nucleophilic cysteine by water-mediated hydrogen bonds (Figures 2 and 3). The PTP10D–GP4 structure further suggests that the active site caves in to trap the substrate. This involves movement of the WPD loop to bring the acid Asp210 (Asp181 in PTP1B and Asp194 in YopH) closer to Cys242 (Cys215 in PTP1B and Cys241 in YopH). The incoming phosphotyrosine thus approaches the nucleophilic cysteine, displacing waters W1 and W2 coordinated by Gln286 (Gln262 in PTP1B and Gln284 in YopH) for the second step of catalysis. This observation is also supported by the PTP10D–PNC and PTP10D–vanadate complexes. Consistent with other PTP complexes, the closure of the WPD loop facilitates the conserved phenylalanine (Phe211 in PTP10D and Phe182 in PTP1B) making ring stacking interactions with the bound phosphotyrosine. The phosphotyrosine thus adopts a position at the base of the active site in an orientation perpendicular to that corresponding to the initial stage of entry (stage II in Figure 2). This orientation of the phosphotyrosine is consistent with the substrate trap mutant structures of PTP1B and YopH (PDB entries 1G1G and 1PA9). This reorientation of the phosphotyrosine ring is important for the coordinated movement of Asp210, allowing Cys242 to complete the formation of the cysteinyl–phosphate intermediate. The movement of the product (dephosphorylated tyrosine) perhaps triggers the waters trapped by the Gln286 (Q loop) to be used for the hydrolysis of the cysteinyl–phosphate intermediate.

A comparison of PTP10D with PTP sequences from *Homo sapiens*, *D. melanogaster*, and *Caenorhabditis elegans* suggests Phe76 is part of the phosphotyrosine recognition (KNRY) loop (Table 1 and Figures S3 and S4 of the Supporting Information). This comparison across 75 PTP sequences (Figure S4 of the Supporting Information) shows the last position of the KNRY loop is either a tyrosine or phenylalanine in 67% of the sequences. The sequences that do not harbor aromatic residues at this position belong to either the membrane distal domains of double-domain RPTPs or pseudophosphatases, both of which are inactive. The absence of this aromatic residue along with mutations in the Asp of the WPD loop is thought to be the reason for the lack of activity in these domains.[4,13] While the role of Asp as the general acid has been well studied, the role of the aromatic residue of the KNRY loop in mediating substrate entry at the PTP active site and facilitating formation of the enzyme–substrate complex has received peripheral attention. The fact that the aromatic residue corresponding to Phe76 is not strictly conserved across PTP homologues was perhaps seen to reflect a less important role for this residue. To biochemically elucidate the role of Phe76 in the dephosphorylation mechanism and kinetics of PTP10D, phosphopeptide and PNC binding experiments were performed with both native PTP10D and its F76L mutant. A decrease in the V_{max} with a corresponding increase in the K_m for the dephosphorylation of the phosphotyrosine-containing peptides without a concomitant change in their peptide sequence preference suggests that Phe76 does not function in substrate selection but affects the reaction rates of phosphatase activity. It thus appears likely that substrate selection occurs at the surface of the active site cavity, whereas Phe76 is involved in the subsequent steps after peptide binding at the active site. The kinetic time course experiments allow an estimate of the role of Phe76 in the reaction mechanism of PTP10D. A PTP-catalyzed reaction can be represented by the following equations:

$$E + RO(PO_3^{2-}) \leftrightarrow [E - O(PO_3^{2-})] + R{-}H \quad (6)$$

$$E + RO(PO_3^{2-}) \rightarrow E + PO_4^{3-} \quad (7)$$

The rate of the formation of the cysteinyl–phosphate enzyme intermediate (eq 6) is defined by a forward rate constant k_1 and

a reverse rate constant k_{-1}. The rate of eq 7 is defined by a forward rate constant k_2. The overall rate is thus

$$k_3 = k_1 - k_{-1} + k_2 \quad (8)$$

The rate of the reverse reaction of the dissociation of the ES complex [E−P(OR)] is negligible at saturating substrate concentrations in the time course experiments. The forward reaction, under these experimental conditions, thus depends only on the rates k_1 and k_2. While the rate of ES complex dissociation to release the free enzyme and the product depends on the catalytic residues (Cys, Asp, and Gln), the rate of ES complex formation (k_1) depends on residues that mediate intermediate formation. A decrease in the V_{max} for all substrates in the case of the F76L mutant suggests that Phe76 affects k_2 of the PTP10D-catalyzed reaction. An overall decrease in the rate of the time course (λ) in the F76L mutant for the five substrates suggests that the F76L mutation also affects rate constant k_1. Phe76 thus serves as a mediating residue that facilitates ES complex formation (Tables 3 and 4).

Binding of PNC at the PTP10D active site depends on two features: electrostatic interactions mediated by the nucleophilic cysteine[34] and the water network at the PTP active site.[25] Mutations of conserved Cys242 lead to a decrease in the rate of binding of PNC at the active site, which is seen by the lower rates (β) for the C242S and C242S/Q286A mutants (Table 4). A decreased lag time and $t_{1/2}$ noted in the case of the D210A/Q286A mutant can probably be rationalized on the basis of the disruption of the water network without any change in the electrostatic environment because of the active site cysteine. Mutation of Phe76, which disrupts neither the nucleophile nor the water network, shows a lag of 160 s and an increased $t_{1/2}$ of PNC binding by 130 s. This suggests that Phe76 plays a role in helping the aryl ring of the substrate progress toward the PTP active site, displacing the water molecules and eventually docking at the nucleophilic cysteine. In the absence of a navigating phenyl group, the substrate ring is likely to adopt multiple conformations, most of which would hinder proper entry of the phosphotyrosine into the active site. The effect on PNC binding kinetics seen in the case of F76L with an increase in the lag time and $t_{1/2}$ is consistent with the role of Phe76 at the step of ES complex formation. These observations are consistent with biochemical studies and molecular dynamics simulations on two membrane-associated receptor PTPs, PTP99A and DLAR, reported recently. These proteins have two PTP domains, D1 and D2. The membrane distal D2 domain is inactive.[40] This observation can be correlated with a mutation of the aromatic residue in the KNRY motif of the D2 domain (Table 1 of the Supporting Information).

To conclude, the structural and biochemical analysis of PTP10D reveals a hitherto unexpected observation of substrate recognition in this class of enzymes. These studies suggest specific roles for relatively less conserved residues that lie at the periphery of the active site in substrate recruitment and modulation of catalytic activity. It thus appears likely that a nuanced regulation of catalytic activity in PTPs occurs at the substrate recruitment stage, in addition to the other characterized mechanisms such as redox sensitivity or oligomerization.

■ ASSOCIATED CONTENT

Supporting Information

Details of the PTP sequence motifs (Table 1) and additional biochemical data, representative sections of electron density, and sequence and structural analysis (Figures S1−S10). This material is available free of charge via the Internet at http://pubs.acs.org.

■ AUTHOR INFORMATION

Corresponding Author

*Lab 301, Molecular Biophysics Unit, Indian Institute of Science, Bangalore 560012, India. Phone: +91-80-229-3219. Fax: +91-80-2360-0535. E-mail: bgopal@mbu.iisc.ernet.in.

Funding

This work was supported by a grant from the Department of Science and Technology, Government of India.

■ ABBREVIATIONS

PTP, protein tyrosine phosphatase; IPTG, isopropyl β-D-thiogalactoside; LB, Luria-Bertani; *p*NPP, *p*-nitrophenyl phosphate; PNC, *p*-nitrocatechol sulfate; rmsd, root-mean-square deviation.

■ REFERENCES

(1) Hunter, T. (2000) Signaling: 2000 and beyond. *Cell 100*, 113−127.

(2) Hunter, T. (1995) Protein kinases and phosphatases: The yin and yang of protein phosphorylation and signaling. *Cell 80*, 225−236.

(3) Fischer, E. H. (1999) Cell signaling by protein tyrosine phosphorylation. *Adv. Enzyme Regul. 39*, 359−369.

(4) Andersen, J. N., Mortensen, O. H., Peters, G. H., Drake, P. G., Iversen, L. F., Olsen, O. H., Jansen, P. G., Andersen, H. S., Tonks, N. K., and Moller, N. P. (2001) Structural and evolutionary relationships among protein tyrosine phosphatase domains. *Mol. Cell. Biol. 21*, 7117−7136.

(5) Desai, C. J., Sun, Q., and Zinn, K. (1997) Tyrosine phosphorylation and axon guidance: Of mice and flies. *Curr. Opin. Neurobiol. 7*, 70−74.

(6) Morrison, D. K., Murakami, M. S., and Cleghon, V. (2000) Protein kinases and phosphatases in the *Drosophila* genome. *J. Cell Biol. 150*, F57−F62.

(7) Schindelholz, B., Knirr, M., Warrior, R., and Zinn, K. (2001) Regulation of CNS and motor axon guidance in *Drosophila* by the receptor tyrosine phosphatase DPTP52F. *Development 128*, 4371−4382.

(8) Tian, S. S., Tsoulfas, P., and Zinn, K. (1991) Three receptor-linked protein-tyrosine phosphatases are selectively expressed on central nervous system axons in the *Drosophila* embryo. *Cell 67*, 675−685.

(9) Yang, X. H., Seow, K. T., Bahri, S. M., Oon, S. H., and Chia, W. (1991) Two *Drosophila* receptor-like tyrosine phosphatase genes are expressed in a subset of developing axons and pioneer neurons in the embryonic CNS. *Cell 67*, 661−673.

(10) Sun, Q., Bahri, S., Schmid, A., Chia, W., and Zinn, K. (2000) Receptor tyrosine phosphatases regulate axon guidance across the midline of the *Drosophila* embryo. *Development 127*, 801−812.

(11) Qian, M., Pan, G., Sun, L., Feng, C., Xie, Z., Tully, T., and Zhong, Y. (2007) Receptor-like tyrosine phosphatase PTP10D is required for long-term memory in *Drosophila*. *J. Neurosci. 27*, 4396−4402.

(12) Dillet, V., Van Etten, R. L., and Bashford, D. (2000) Stabilization of Charges and Protonation States in the Active Site of the Protein Tyrosine Phosphatases: A Computational Study. *J. Phys. Chem. B 104*, 11321−11333.

(13) Zhang, Z. Y. (1998) Protein-tyrosine phosphatases: Biological function, structural characteristics, and mechanism of catalysis. *Crit. Rev. Biochem. Mol. Biol. 33*, 1−52.

(14) Zhang, Z. Y. (2002) Protein tyrosine phosphatases: Structure and function, substrate specificity, and inhibitor development. *Annu. Rev. Pharmacol. Toxicol. 42*, 209−234.

(15) Fashena, S. J., and Zinn, K. (1997) Transmembrane glycoprotein gp150 is a substrate for receptor tyrosine phosphatase DPTP10D in *Drosophila* cells. *Mol. Cell. Biol. 17*, 6859−6867.
(16) Powell, H. R. (1999) The Rossmann Fourier autoindexing algorithm in MOSFLM. *Acta Crystallogr. D55*, 1690−1695.
(17) Evans, P. (2006) Scaling and assessment of data quality. *Acta Crystallogr. D62*, 72−82.
(18) McCoy, A. J., Grosse-Kunstleve, R. W., Storoni, L. C., and Read, R. J. (2005) Likelihood-enhanced fast translation functions. *Acta Crystallogr. D61*, 458−464.
(19) Storoni, L. C., McCoy, A. J., and Read, R. J. (2004) Likelihood-enhanced fast rotation functions. *Acta Crystallogr. D60*, 432−438.
(20) Stein, N. (2008) CHAINSAW: A program for mutating pdb files used as templates in molecular replacement. *J. Appl. Crystallogr. 41*, 641−643.
(21) Murshudov, G. N., Vagin, A. A., and Dodson, E. J. (1997) Refinement of macromolecular structures by the maximum-likelihood method. *Acta Crystallogr. D53*, 240−255.
(22) Emsley, P., and Cowtan, K. (2004) Coot: Model-building tools for molecular graphics. *Acta Crystallogr. D60*, 2126−2132.
(23) Schuttelkopf, A. W., and van Aalten, D. M. (2004) PRODRG: A tool for high-throughput crystallography of protein-ligand complexes. *Acta Crystallogr. D60*, 1355−1363.
(24) Davis, I. W., Leaver-Fay, A., Chen, V. B., Block, J. N., Kapral, G. J., Wang, X., Murray, L. W., Arendall, W. B. III, Snoeyink, J., Richardson, J. S., and Richardson, D. C. (2007) MolProbity: All-atom contacts and structure validation for proteins and nucleic acids. *Nucleic Acids Res. 35*, W375−W383.
(25) Vriend, G. (1990) WHAT IF: A molecular modeling and drug design program. *J. Mol. Graphics 8*, 29 , 52−56.
(26) Collaborative Computational Project, Number 4 (1994) The CCP4 suite: Programs for protein crystallography. *Acta Crystallogr. D50*, 760−763.
(27) Pettit, F. K., Bare, E., Tsai, A., and Bowie, J. U. (2007) HotPatch: A statistical approach to finding biologically relevant features on protein surfaces. *J. Mol. Biol. 369*, 863−879.
(28) Waterhouse, A. M., Procter, J. B., Martin, D. M., Clamp, M., and Barton, G. J. (2009) Jalview Version 2: A multiple sequence alignment editor and analysis workbench. *Bioinformatics 25*, 1189−1191.
(29) Madan, L. L., and Gopal, B. (2008) Addition of a polypeptide stretch at the N-terminus improves the expression, stability and solubility of recombinant protein tyrosine phosphatases from *Drosophila melanogaster*. *Protein Expression Purif. 57*, 234−243.
(30) Geladopoulos, T. P., Sotiroudis, T. G., and Evangelopoulos, A. E. (1991) A malachite green colorimetric assay for protein phosphatase activity. *Anal. Biochem. 192*, 112−116.
(31) Kakkar, T., Boxenbaum, H., and Mayersohn, M. (1999) Estimation of K_i in a competitive enzyme-inhibition model: Comparisons among three methods of data analysis. *Drug Metab. Dispos. 27*, 756−762.
(32) Khajehpour, M., Wu, L., Liu, S., Zhadin, N., Zhang, Z. Y., and Callender, R. (2007) Loop dynamics and ligand binding kinetics in the reaction catalyzed by the *Yersinia* protein tyrosine phosphatase. *Biochemistry 46*, 4370−4378.
(33) Pedersen, A. K., Peters, G. G., Moller, K. B., Iversen, L. F., and Kastrup, J. S. (2004) Water-molecule network and active-site flexibility of apo protein tyrosine phosphatase 1B. *Acta Crystallogr. D60*, 1527−1534.
(34) Sun, J. P., Wu, L., Fedorov, A. A., Almo, S. C., and Zhang, Z. Y. (2003) Crystal structure of the *Yersinia* protein-tyrosine phosphatase YopH complexed with a specific small molecule inhibitor. *J. Biol. Chem. 278*, 33392−33399.
(35) Salmeen, A., Andersen, J. N., Myers, M. P., Tonks, N. K., and Barford, D. (2000) Molecular basis for the dephosphorylation of the activation segment of the insulin receptor by protein tyrosine phosphatase 1B. *Mol. Cell 6*, 1401−1412.
(36) Jia, Z., Barford, D., Flint, A., and Tonks, N. (1995) Structural basis for phosphotyrosine peptide recognition by protein tyrosine phosphatase 1B. *Science 268*, 1754−1758.
(37) Tsiani, E., Bogdanovic, E., Sorisky, A., Nagy, L., and Fantus, I. G. (1998) Tyrosine phosphatase inhibitors, vanadate and pervanadate, stimulate glucose transport and GLUT translocation in muscle cells by a mechanism independent of phosphatidylinositol 3-kinase and protein kinase C. *Diabetes 47*, 1676−1686.
(38) Huyer, G., Liu, S., Kelly, J., Moffat, J., Payette, P., Kennedy, B., Tsaprailis, G., Gresser, M. J., and Ramachandran, C. (1997) Mechanism of inhibition of protein-tyrosine phosphatases by vanadate and pervanadate. *J. Biol. Chem. 272*, 843−851.
(39) Xie, L., Zhang, Y. L., and Zhang, Z. Y. (2002) Design and characterization of an improved protein tyrosine phosphatase substrate-trapping mutant. *Biochemistry 41*, 4032−4039.
(40) Madan, L. L., Veeranna, S., Shameer, K., Reddy, C. C. S., Sowdhamini, R., and Gopal, B. (2011) Modulation of Catalytic Activity in Multi-Domain Protein Tyrosine Phosphatases. *PLoS One 6*, e24766.